Published August 23, 2018

Original Research

Core Ideas

- Parameterized models are relevant to applications where different porous media mixtures are used.
- Models include a grain-size distribution function to describe bimodal behavior for binary mixtures.
- Improved model describes observed thermal conductivity–saturation relations for binary mixtures.
- Combined Buckingham–Penman model used to describe observed gas diffusivity–air content relations.
- This work is relevant for proper simulation of mixed porous media.

Characterization of Grain-Size Distribution, Thermal Conductivity, and Gas Diffusivity in Variably Saturated Binary Sand Mixtures

T.K.K. Chamindu Deepagoda, Kathleen Smits,* J.R.R.N. Jayarathne, Benjamin M. Wallen, and Timothy J. Clough

Characterization of differently textured porous materials, as well as different volumetric porous media mixtures, in relation to mass and heat transport is vital for many engineering and research applications. Functional relations describing physical (e.g., grain-size distribution, total porosity), thermal, and gas diffusion properties of porous media and mixtures are necessary to optimize the design of porous systems that involve heat and gas transport processes. However, only a limited number of studies provide characterization of soil physical, thermal, and gas diffusion properties and the functional relationships of these properties under varying soil water contents, especially for soil mixtures, complicating optimization efforts. To better understand how mixing controls the physical, thermal, and gas diffusion properties of porous media, a set of laboratory experiments was performed using five volumetric mixtures of coarse- and fine-grained sand particles. For each mixture, the grain-size distribution (GSD), thermal conductivity, and gas diffusivity were obtained and parameterized using existing and suggested parametric models. Results show that the extended, two-region Rosin–Rammler particle-size distribution model proposed in this study could successfully describe the bimodal behavior of the GSD of binary mixtures. Further, the modified Côté and Konrad thermal conductivity model adequately described the thermal conductivity–water saturation relations observed in different mixtures. The proposed simple soil-gas diffusivity descriptive model parameterized the upper limit, average, and lower limit behavior in gas diffusivity–air content relations in apparently texture-invariant gas diffusivity data. Results further show a close analogy between gas diffusivity and thermal conductivity and their variation with saturation across different binary mixtures. Overall, the results of the study provide useful numerical insight into the physical, thermal, and gas transport characteristics of binary mixtures, with wide implications for future engineering and research applications that involve multicomponent porous systems.

Abbreviations: C-K, Côté and Konrad; GSD, grain-size distribution.

T.K.K. Chamindu Deepagoda, Dep. of Civil Engineering, Univ. of Peradeniya, 20400 Peradeniya, Sri Lanka; K. Smits, Dep. of Civil Engineering, Univ. of Texas, Arlington, TX 76019; J.R.R.N. Jayarathne, Dep. of Civil Engineering, Univ. of Peradeniya, 20400 Peradeniya, Sri Lanka; B.M. Wallen, Dep. of Geography and Environmental Engineering, US Military Academy, West Point, NY 10996; T.K.K. Chamindu Deepagoda and T.J. Clough, Dep. of Soil and Physical Sciences, Lincoln Univ., P.O. Box 85084, Lincoln 7647, New Zealand. *Corresponding author (ksmits@mines.edu).

Received 30 Jan. 2018.
Accepted 23 May 2018.

Citation: Chamindu Deepagoda, T.K.K., K. Smits, J.R.R.N. Jayarathne, B.M. Wallen, and T.J. Clough. 2018. Characterization of grain-size distribution, thermal conductivity, and gas diffusivity in variably saturated binary sand mixtures. Vadose Zone J. 17:180026. doi:10.2136/vzj2018.01.0026

Characterizing mass and energy transport processes in variably saturated porous media is of great importance due to the wide application of these processes in natural and engineered porous systems. In particular, porous beds packed with pre-characterized materials enable controlled transfer of mass and energy through engineered systems, and therefore they are common in industrial and research-based applications. For example, sand-packed filters with known hydraulic properties are extensively used in traditional water and wastewater treatment plants for removal of particulate substances during the purification process. Similarly, biofilters fitted with packed-bed units are widely used for efficient removal of gaseous pollutants from industrial emissions (Delhoménie and Heitz, 2005). Also, porous media heat exchangers using differently characterized porous materials are common in process industries for heat (thermal energy) transfer with high efficiency (Delavar and Azimi, 2013). In addition, some engineering applications enable coupled flow through packed porous media, for example the gas and heat flow through gas heat exchanger

units used in drying or cooling industries (Pavel and Mohamad, 2004). Porous media used in these engineering applications differ largely with respect to grain size and size distribution, other physical characteristics, as well as the transport properties of interest.

Apart from engineering applications, pre-characterized porous materials and their mixtures are also used in research studies to investigate single- or multiphase fate and transport of mass and energy in porous media. Porous media with known characteristics are widely used in research for conceptual and mechanistic model development, testing of new apparatus and sensor technology, validation of computer simulations, etc. Conceptual and numerical characterizations of transport in multicomponent porous media systems, including binary granular mixtures, have been presented in the literature in relation to electrical, hydrodynamic, and thermal properties (e.g., Lemaitre et al., 1988; Mota et al., 2001; Dias et al., 2004).

Despite their wide application to engineering and research studies, there are very few studies that present the detailed characteristic and functional relationships of pre-characterized materials, especially for soil mixtures. Most previous studies related to soil mixtures focus on soil hydraulic properties (e.g., soil water retention and hydraulic conductivity) but provide little insight into soil thermal and diffusive properties. Although this may be appropriate for many applications, engineered systems and research studies focusing on heat and mass transport, like those described above, require detailed knowledge of additional soil characteristics to maximize optimization efforts.

Although much effort has been invested in the development of functional relationships for soil thermal conductivity–water content (e.g., de Vries, 1963; Johansen, 1975; Campbell, 1985; Tarnawski et al., 2013; Lu et al., 2007; Chen, 2008; Côté and Konrad, 2005; Lu and Dong, 2015) and gas diffusivity–air content (e.g., Buckingham, 1904; Penman, 1940; Millington and Quirk, 1961; Moldrup et al., 2000), none of the models specifically addresses the applicability to soil mixtures. Recently, Wallen et al. (2016) evaluated the applicability of different soil thermal conductivity–soil moisture models to soil mixtures. The models fit experimental data to varying degrees based on the number of parameters used, demonstrating the need for a modified thermal conductivity–water content model for soil mixtures. Pokhrel et al. (2011) studied the gas diffusivity–air content relation in different soil–compost mixtures to be applied in gas-phase biofilters. They highlighted the limited applicability of widely used predictive models to accurately describe gas diffusivity in soil–compost mixtures.

To better understand how mixing controls soil thermal and diffusive properties, a set of laboratory experiments was performed in this study using binary mixtures of coarse- and fine-grained particles. We characterized and parameterized the GSD, thermal conductivity, and gas diffusivity in seven volumetric mixtures of two sand grades: a coarse-grained sand (no. 12/20) and a fine-grained sand (no. 110). The two sands were selected due to their extensive use across the world for a range of applications in research, such as soil model comparisons (Sakaki and Illangasekare, 2007; Sweijen et al., 2017), gas kinetics studies (Taylor and Kwan, 2004), oil recovery enhancement investigations (Donaldson et al., 1985), infiltration studies (DiCarlo, 2004), nonaqueous-phase liquid plume migration studies (Abriola et al., 2013), and pore structure visualization studies (e.g., Hamamoto et al., 2016).

We note here that Sakaki and Smits (2015) previously studied the water retention characteristics of the same sand mixtures, while this study extends the analysis also to soil physical, thermal, and gas diffusion characteristics. Thus, this study, combined with that of Sakaki and Smits (2015), provides a complete set of soil properties and functional relationships that will be useful for future engineering and research applications where similar sand grades and mixtures are used.

Materials and Methods

Sand Materials

In this study, we used two uniform specialty silica sand grades: no. 12/20 (identified by the effective sieve number) (Accusand, Unimin Corporation), and no. 110 (Ottawa sand, US Silica Co.). Figure 1 shows the textural contrast of the two sand types.

These well-processed sands were selected due to their high batch-to-batch consistency, wide commercial availability, and widespread use in engineering and research-based applications. The sand mineralogy is characterized as 99.8% quartz, which yielded a grain density of 2.66 g cm^{-3}. The chemical composition of the sands was detailed by Schroth et al. (1996). The high sphericity (e.g., 0.9 for no. 12/20 sand; Schroth et al., 1996) of sand grains, and thus the consistency of samples in replicate packing, is another important property that makes the sands a suitable porous medium for a wide range of research applications. The sands also have high uniformity coefficients (1.7 and 1.2 for no. 12/20 and 110, respectively), allowing consistently reproducible results. Due to high purity (with a negligibly small amount of organic matter), the sands require no additional treatments prior to use in experiments. The basic properties of the two sands and the five gravimetric mixtures used in this study are shown in Table 1.

Methods

In addition to the two component sands, mass-weighted fractions of each component were uniformly mixed to produce, in total,

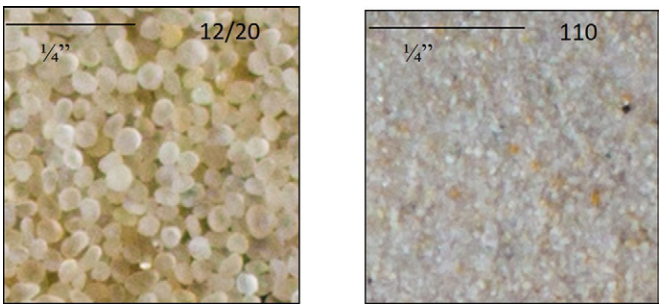

Fig. 1. Two differently textured sand types considered for characterization: no. 12/20 (left), and no. 110 (right) (horizontal scale: 0.635 cm [1/4 inch]).

Table 1. Physical properties of the binary mixtures used in this study.

Porous medium†	Avg. particle diameter (D_{50})	Total porosity	Bulk density	Water retention properties		Thermal conductivity (λ)		$D_{p,dry}/D_o$§
				Air-entry pressure‡	Residual water content	λ_{dry}	λ_{sat}	
	mm	$cm^3\ cm^{-3}$	$g\ cm^{-3}$	cm H_2O	$cm^3\ cm^{-3}$	——— $W\ m^{-1}\ K^{-1}$ ———		
C10F0	1.03	0.318	1.81	10.8	0.004	0.287	3.383	0.161
C9F1	1.02	0.261	1.96	10.7	0.013	0.427	4.396	NA¶
C8F2	1.01	0.212	2.09	10.5	0.015	0.558	4.833	0.129
C7F3	0.97	0.190	2.15	52.1	0.006	0.529	5.010	NA
C5F5	0.57	0.237	2.02	72	0.007	0.419	4.851	0.117
C2F8	0.15	0.298	1.86	78	0.007	0.332	3.947	0.099
C0F10	0.14	0.337	1.76	72.8	0	0.282	3.241	0.166

† Mixtures are named as the ratio of coarse (C) to fine (F) grain size.
‡ 10 cm $H_2O \approx 1$ kPa.
§ *G*as diffusivity at complete air saturation.
¶ NA, not available.

seven different coarse-to-fine (C/F) mixtures: 10:0, 9:1, 8:2, 7:3, 5:5, 2:8, and 0:10. The mixtures are referred to as C10F0, C9F1, C8F2, C7F3, C5F5, C2F8, and C0F10, respectively, following the nomenclature of Wallen et al. (2016) and Sakaki and Smits (2015). Grain-size distributions of the seven mixtures were obtained following sieve analysis (data from Wallen et al., 2016).

Thermal conductivity measurements performed by Smits et al. (2010, 2012) were used for the numerical characterizations. The measurements were performed in a small cell apparatus (9 cm in height and 8.8 cm o.d.) in which capillary pressure was regulated by a hydraulically connected 200-cm-high hanging water reservoir. Measurements for soil moisture (ECH_2O EC-5, Decagon Devices), thermal conductivity (SH-1, Decagon Devices), and capillary pressure (porous cup tensiometer, Soilmoisture Equipment Corp.) were performed using corresponding sensors at different moisture statuses. The initially wet-packed cell was subjected to stepwise draining to the intended bulk density (see Table 1), followed by successive draining to specific matric suctions by regulating the water level of the reservoir. Smits et al. (2012) provided a detailed description of the experimental procedure and sensor specifications, together with a schematic presentation of the experimental setup.

Gas diffusivity (D_p/D_o) measurements (where D_p and D_o are gas diffusion coefficients in soil and free air, respectively) were conducted for the selected mixtures of this study. For D_p/D_o measurements, we used the one-chamber diffusion cell apparatus introduced by Taylor (1950) and modified further by Schjønning (1985). The diffusion chamber was constructed out of a 10-mm-thick polyvinyl chloride tube (3.14-cm i.d. and 10-cm height), embedded and glued into a 10-mm-thick plastic bottom plate. To facilitate sample positioning and to ensure an airtight joint, a 5-cm-diameter rubber O-ring was embedded into an engraved slot at the top edge of the tube. An oxygen sensor (KE-25, Figaro Inc.) was outfitted at the mid-height of the cell wall for O_2 measurements. Two valves were placed at the top and bottom of the cell to facilitate N_2 flushing. Before initiating a series of measurements, a preliminary diffusion test was conducted to confirm the airtightness of the chamber.

Annular metal sampling cores (6.06 cm in diameter and 3.48 cm in height; ~100 cm^3 in volume) were uniformly packed in triplicate to the intended bulk densities (Table 1). Saturated samples were exposed to controlled evaporation, and diffusivity measurements were conducted at different moisture conditions after evaporation. After each measurement, the samples were kept closed for several hours to allow water redistribution before the next measurement.

The chamber was first flushed with N_2 to create an O_2–free chamber. Then the sample was mounted on the top of the chamber and exposed to the atmosphere, thus permitting O_2 to diffuse from the atmosphere into the chamber through the sample. The increasing O_2 concentration inside the chamber was recorded using a datalogger (National Instruments Corp.) and monitored via a LabVIEW interface (National Instruments Corp.). For the calculations of the diffusion coefficient, we used the Currie (1960) method as outlined by Rolston and Moldrup (2002).

During sampling preparations and packing for both thermal conductivity and gas diffusivity measurements, we followed an identical procedure for all mixing proportions. We did not specifically control porosity or density and allowed the porosity and density to change with each mixing proportion to investigate the effect of binary mixing on porosity and density and, in turn, also on gas diffusivity and thermal conductivity. Because gas diffusivity, in particular, is more a porosity-controlled parameter than a texture-controlled parameter (Moldrup et al., 2000), we hypothesized that the ensuing effects of mixing on the total porosity would be reflected in the results.

Numerical Modeling

Grain-Size Distribution

For GSD modeling, the classical Rosin–Rammler distribution function (Rosin and Rammler, 1933), originally developed

for unimodal type grain-size distributions, is invoked. The function essentially parameterizes the percentage passing (by weight) of particles, P (%), expressed as a function of grain size, x (mm), using two fitting coefficients:

$$P(x)=100\left\{1-\exp\left[-\left(\frac{x}{\alpha}\right)^{\beta}\right]\right\} \quad [1]$$

where α (μm) and β (dimensionless) are model fitting coefficients representing the characteristic size and the spread of the grain-size distribution, respectively. Note that the characteristic size (α) corresponds to the 63rd percentile of the distribution (i.e., P = 63% when $x = \alpha$).

To numerically describe the bimodal type grain-size distributions, as observed for different binary mixtures, we extended Eq. [1] to a two-region grain size distribution function, with an implicit hypothesis that the unimodal grain-size distribution functions of the two sands are algebraically additive:

$$P(X)=100\left(\omega\left\{1-\exp\left[-\left(\frac{x}{\alpha_f}\right)^{\beta_f}\right]\right\}+(1-\omega)\left\{1-\exp\left[-\left(\frac{x}{\alpha_c}\right)^{\beta_c}\right]\right\}\right) \quad [2]$$

wherein α_f (μm) and α_c (μm) are characteristic sizes (63rd percentile values) representing the fine and coarse size distributions, respectively; and β_f (dimensionless) and β_c (dimensionless) are corresponding coefficients representing the spread of the distributions. The weighted mass fraction of the fine sand, w (dimensionless), is also used as a fitting coefficient together with above parameters.

Differentiating Eq. [1] and [2] yields grain size density functions, $p(x)$ ($=\partial[P(x)]/\partial x$), representing unimodal (Eq. [3]) and bimodal (Eq. [4]) conditions:

$$p(x)=100\exp\left[-\left(\frac{x}{\alpha}\right)^{\beta}\right]\left(\frac{x}{\beta}\right)^{\beta-1}\left(\frac{\beta}{\alpha}\right) \quad [3]$$

$$p(x)=100\left\{\omega\exp\left[-\left(\frac{x}{\alpha_f}\right)^{\beta_f}\right]\left(\frac{x}{\alpha_f}\right)^{\beta_f-1}\left(\frac{\beta_f}{\alpha_f}\right)+(1-\omega)\exp\left[-\left(\frac{x}{\alpha_c}\right)^{\beta_c}\right]\left(\frac{x}{\alpha_c}\right)^{\beta_c-1}\left(\frac{\beta_c}{\alpha_c}\right)\right\} \quad [4]$$

When only one sand type (fine-grained or coarse-grained) is present in the mixture (i.e., w = 1 or 0), Eq. [4] reduces to Eq. [3].

Note also that $p(x)$, being a density function, yields unity when it is integrated over the entire space:

$$\int_0^{\infty} p(x)=1 \quad [5]$$

The locations of the peaks can also be derived from the second derivative of $p(x)$, leading to

$$\left(\frac{1}{\alpha_f}\right)\exp\left[-\left(\frac{x}{\alpha_f}\right)^{\beta_f}\right]\left[\left(\beta_f-1\right)\left(\frac{x}{\alpha_f}\right)^{\beta_f-2}-\beta_f\left(\frac{x}{\alpha_f}\right)^{2\beta_f-2}\right]=0$$

$$\left(\frac{x}{\alpha_f}\right)^{\beta_f-2}\left[\left(\beta_f-1\right)-\beta_f\left(\frac{x}{\alpha_f}\right)^{\beta_f}\right]=0$$

$$\beta_f\left(\frac{x}{\alpha_f}\right)^{\beta_f}=\beta_f-1 \quad [6]$$

$$\frac{x}{\alpha_f}=\left[\frac{\beta_f-1}{\beta_f}\right]^{1/\beta_f}$$

yielding

$$x_f=\alpha_f\left[1-\frac{1}{\beta_f}\right]^{1/\beta_f} \quad \beta_f\geq 1 \quad [7]$$

where x_f (mm) corresponds to the median size of the finer fraction (hence the peak in the density function). Note that x_f/α_f (i.e., the measure of grain size uniformity between the 50th and 63rd percentile grain-size distribution) is a highly nonlinear function of β_f, with $x_f/\alpha_f = 0$ when $\beta_f = 1$ and $x_f/\alpha_f = 1$ as β_f reaches infinity. The larger β_f yields a more uniform distribution. A similar function can be written for the distribution of the coarse size fraction as well. Figure 2 demonstrates the locations of the two peaks in a typical grain-size density distribution as derived by Eq. [7].

Thermal Conductivity

The literature is abundant with a wide range of models that provide the soil thermal conductivity (λ, W m^{-1} K^{-1})–water saturation ($S = \theta/\Phi$; where θ is water content [cm^3 cm^{-3}] and Φ [cm^3 cm^{-3}] is porosity) relationships (e.g., de Vries, 1963; Johansen, 1975; Campbell et al., 1994; Côté and Konrad, 2005; Chen, 2008; Haigh, 2012, Lu and Dong, 2015). In a recent study, Chamindu Deepagoda et al. (2016) revisited the Côté and Konrad (2005) model (C-K) to explain different thermal regimes identified in uniform sand grades. They expanded the original C-K model to a multiparameter multiregion function, with each parameter characterizing the distinct regions (defined below) observed in the characteristic λ–S curve. The original C-K model takes the form

$$\lambda(K_e)=\left(\lambda_{sat}-\lambda_{dry}\right)K_e+\lambda_{dry}$$

$$K_e(S)=\frac{kS}{1+(k-1)S} \quad 0\leq S\leq 1 \quad [8]$$

where λ_{dry} and λ_{sat} (W m^{-1} K^{-1}) are thermal conductivities in soil under completely dry and fully water-saturated conditions,

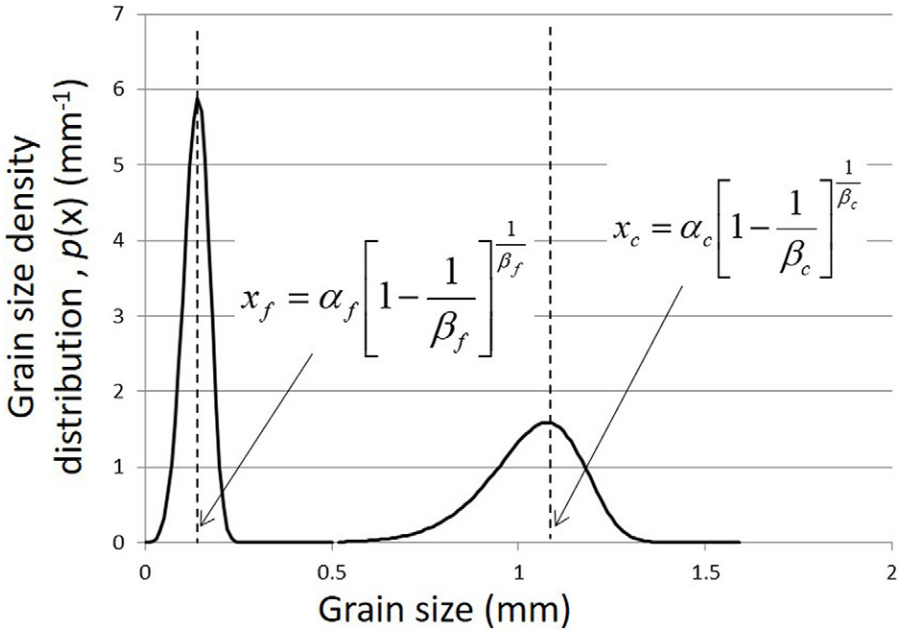

Fig. 2. Illustration of the grain-size density function (Eq. [3] and [4]) and locations of the peaks for fine-textured and coarse-textured sand grades; x_f and x_c correspond to the median size of the fine and coarse fractions, respectively; α_f and α_c are 63rd percentile values representing the fine and coarse size distributions, respectively; β_f and β_c are corresponding coefficients representing the spread of the distributions.

respectively; K_e is the so-called Kersten number, and k is a fitting parameter considered as descriptive of the grain-size distribution, pore size, and pore water content (Côté and Konrad, 2005). The values for λ_{dry} and λ_{sat} are either measured or inversely estimated using the model. In this study, we measured both λ_{dry} and λ_{sat} (see Table 1) values and used them as model-constraining parameters in λ–S relations.

The modified Kersten number from Chamindu Deepagoda et al. (2016) can be written as

$$\lambda\left(K_{e,i}\right)=\begin{cases}\left(\lambda_f-\lambda_{dry}\right)K_{e,i}+\lambda_{dry} & 0\le S\le S_0 \text{ and } S_f\le S\le 1\\ \left(\lambda_{sat}-\lambda_f\right)K_{e,i}+\lambda_f & S_0\le S\le S_f\end{cases} \quad [9]$$

where $K_{e,i}$ (i = 0,1,2) represent the Kersten numbers assigned to three saturation regions, $0 \le S \le S_0$ (i = 0), $0 \le S \le S_f$ (i = 1), and $S_f \le S \le 1$ (i = 2), wherein thermal conductivity behavior varies markedly. The parameters were defined in such a way that λ_f (W m^{-1} K^{-1}) denotes the thermal conductivity corresponding to S_f, the saturation that marks the termination of the sharp increase in thermal conductivity that started from saturation S_0. The two saturation points characterizing the transition, S_f and S_0, are difficult to estimate experimentally. In this study, the two parameters were estimated inversely by parameter optimization.

The region-dependent Kersten number, $K_{e,i}$, for each saturation region was defined as

Region 0 (constant region)

$$K_{e,0}=0 \quad 0\le S\le S_0 \quad [10]$$

Region 1 (linear region)

$$K_{e,1}=\frac{S-S_0}{S_f-S_0} \quad S_0\le S\le S_f \quad [11]$$

Region 2 (nonlinear region)

$$K_{e,2}(S)=\frac{k\left(S-S_f\right)}{1-\left[1-k\left(1-S_f\right)\right]S} \quad S_f\le S\le 1 \quad [12]$$

Equation [12] reduces to the original Côté and Konrad (2005) model (Eq. [8]) when S_f = 0 (i.e., when region-based characterization is ignored).

Gas Diffusivity

A wide range of gas diffusivity (D_p/D_o) models are available for characterizing gas diffusion in soils and porous media, which have been developed following theoretical (e.g., Millington, 1959; Millington and Quirk, 1960, 1961), empirical (e.g., Buckingham, 1904; Penman, 1940), semi-conceptual (e.g., Moldrup et al., 2000), and conceptual (e.g., Troeh et al., 1982) modeling approaches. Among those, two pioneering gas diffusivity models are the Buckingham (1904) model:

$$\frac{D_p}{D_o}=\varepsilon^2 \quad [13]$$

and the Penman (1940) model:

$$\frac{D_p}{D_o}=0.66\varepsilon \quad [14]$$

where ε (cm^3 cm^{-3}) is the air-filled porosity. The exponent (= 2) in Eq. [13] and the scaling factor (= 0.66) in Eq. [14] are empirical coefficients. Conceptually, the Penman model violates the fundamental requirement that D_p/D_o should be essentially 1 when ε = 1 (i.e., in a soilless medium), while the Buckingham model has no provision to describe diffusivity in a fractured porous system where the diffusivity increases linearly with air-filled porosity. Considering these drawbacks of the two models, a generalized equation can be written in the form of a combined Buckingham–Penman model:

$$\frac{D_s}{D_o} = A\varepsilon^B \quad [15]$$

where A and B are model parameters characterizing the functional air phase of the porous domain. In fact, a close look at widely used D_p/D_o models reveals that they could be rearranged in the form of Eq. [15] when appropriate values or properties are assigned to the parameters A and B, as demonstrated in Table 2. The table also includes the theoretical upper limit model with the parameter pair (A = 1 and B = 1) showing the least resistance (i.e., the minimum tortuosity and the maximum connectivity) to diffusive gas transport through a porous system.

Results and Discussion

Grain-Size Distribution

The observed and simulated (Eq. [2]) GSDs for the seven mixtures of two sand grades are illustrated in Fig. 3.

The observed data show the clear bimodal variation in the GSD. In model parameterization, we optimized four parameters based on the least squares method. A very good agreement between the observed data and the extended bimodal Rosin–Rammler GSD can be observed, suggesting the applicability of this new modeling approach. There is excellent agreement (R^2 = 0.999) between the measured and model-optimized volumetric fraction (w) as illustrated in Fig. 4. Note that no constraints were applied during the optimization process.

This strong agreement, in turn, successfully tests our hypothesis that the two GSD functions are algebraically additive when representing a uniform mixture of two size distributions. It is important to note that the very good agreement between the observed and simulated results in Fig. 4 does not necessarily imply that the two unimodal functions are additive in nature, since the fitting approach followed here is purely mathematically based, with no physically related constraints. The strong agreement of measured and simulated w values, however, suggests that the model has yielded physically interpretable results. This is supported by the agreement of the α and β values for both size fractions in all mixtures (see Table 3). The extended function, Eq. [2], can therefore be used to simulate the particle-size distribution of any mixture with a known w value, together with the average parameters for α and β values as in Table 2. The function can also be conveniently extended to multimodal distributions, for instance for the uniform mixtures of three or four different grain sizes, as required for a particular research or engineering application.

Figures 5a through 5g show the grain-size density distribution (Eq. [3] and [4]) for the seven sand mixtures. Note the decreasing density (i.e., the peak height) of the coarser grain fraction as that of the finer grain-size density increases, while the grain size (related to α) and the spread (related to β) remain more or less the same for the two size fractions.

Table 2. Gas diffusivity models analogous to the proposed model (Eq. [15]) and corresponding model parameters.

Model	Equation†	$D_p/D_o = A\varepsilon^B$	
		A	B
Theoretical upper limit model (all pores aligned in the direction of flow)	$D_p/D_o = \varepsilon$	1	1
Buckingham (1904)	$D_p/D_o = \varepsilon^2$	1	2.0
Penman (1940)	$D_p/D_o = 0.66\varepsilon$	0.66	1.0
Millington (1959)	$D_p/D_o = \varepsilon^{4/3}$	1	1.33
Marshall (1959)	$D_p/D_o = \varepsilon^{3/2}$	1	1.5
Millington and Quirk (1960)	$D_p/D_o = \varepsilon^2/\Phi^{2/3}$	$\Phi^{-2/3}$	2.0
Millington and Quirk (1961)	$D_p/D_o = \varepsilon^{10/3}/\Phi^2$	Φ^{-2}	3.33
Moldrup et al. (2000) (WLR–Marshall)	$D_p/D_o = \varepsilon^{3/2}(\varepsilon/\Phi)$	Φ^{-1}	2.5
Hamamoto et al. (2009)	$D_p/D_o = \varepsilon^X(\varepsilon/\Phi)^N$	Φ^{-N}	$X + N$
Chamindu Deepagoda et al. (2011)	$D_p/D_o = 0.5\Phi(\varepsilon/\Phi)^\beta$	$0.5\Phi^{-(\beta-1)}$	β

† D_p/D_o, soil-gas diffusivity; ε, air-filled porosity; Φ, total porosity.

Thermal Conductivity

The change in thermal conductivity (λ) across saturation (S) is shown in Fig. 6 for the seven sand grades. Simulations are shown using two λ–S models, Côté and Konrad (Eq. [8], dotted line) and the improved Côté and Konrad model (Eq. [9–12], solid line) together with the measured data (open circles). Clearly, the improved C-K model numerically represented the overall λ–S behavior better than the original C-K model, as the latter tended to mischaracterize the transition between Regions 1 and 2 in the λ–S curve. We note that the sharp changes in the characteristic λ–S curve arise from the uniformity of the particles and distinct size fractions, which impacts the development of bridges facilitating heat transfer with increasing water content at a specific saturation. In natural field soils, due to the presence of a wide spectrum of differently sized and shaped particles, the changes occur gradually across a range of saturations, not at a sharp point. Consequently, natural soils may tend to follow the original C-K model, while the extended model is still applicable with suitably selected parameters.

Figure 7 (left) shows the variation of three λ values, λ_{dry} (measured under completely dry conditions), λ_{sat} (measured under completely water-saturated conditions), and λ_f (representing the partially saturated condition wherein the formation of water bridges, causing a rapid increase in heat transfer, is nearly complete). The variation of total porosity (Φ) with volumetric fraction (w) is also shown (in the secondary y axis) for comparison. All λ values peaked nearly around 30% of fine fractions, exactly at the point where Φ exhibited the minimum, across saturation conditions, thus corroborating previous observations (e.g., Sakaki and Smits, 2015; Wallen et al., 2016). This implies the important inverse relationship between the thermal conductivity and total porosity. As the pore space, occupied by less thermally conductive air (≈0.024 W m^{-1} K^{-1}) and/or water (≈0.580 W m^{-1} K^{-1}), is replaced by high-conductivity quartz (≈7.5 W m^{-1} K^{-1}), the

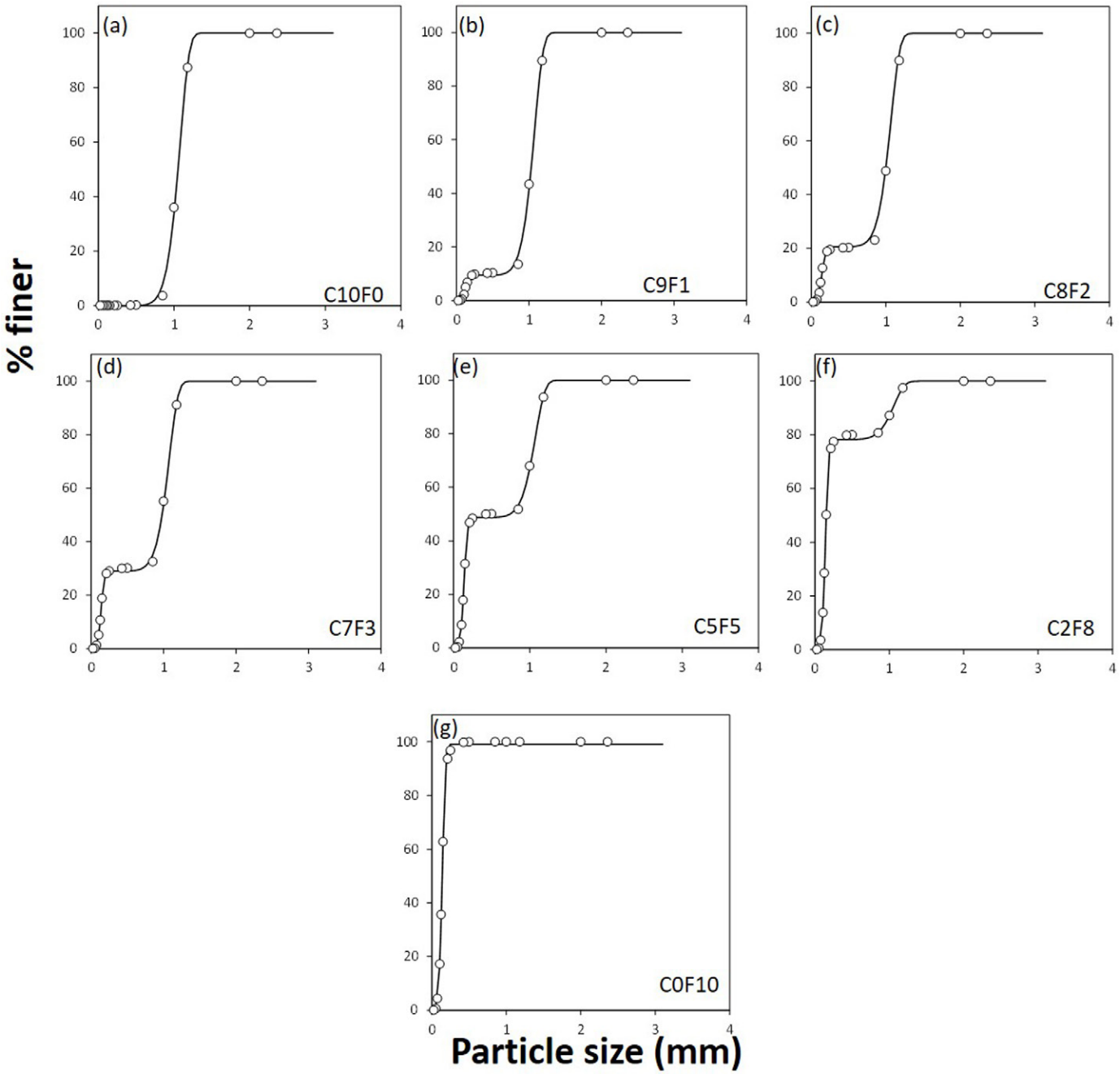

Fig. 3. Grain-size distribution (Eq. [2]) for the seven different binary sand mixtures.

thermal conductivity increases while the porosity decreases. From this evaluation, it is also evident that under the various saturation conditions, the solid content and the associated grain–grain contacts are the main drivers of the thermal conductivity in a homogenous porous medium. However, it should be noted that the two components and grades (no. 12/20 and 110), although markedly different in size, have similar intrinsic thermal conductivities. Therefore, the grain-to-grain contacts between similar sand grades and dissimilar ones behave almost identically with respect to heat transport. Although not supported by the present results, the effect of volumetric proportion could have been seen if the two sand grades in the mixture had different thermal conductivity characteristics. Figure 7 (right) portrays the variation of numerically derived (inversely estimated) parameters, S_0 and S_f, as a function of volumetric fraction. As a reference, the variation in total porosity is also shown. No clear trend could be seen in the variation of S_0 vs. w, however S_f, although not very pronounced, tended to follow a similar variation as observed for λ_f in Fig. 7 (left). Strictly speaking, S_0 and S_f are microscopically related properties and hence may not be able to be accurately derived from the numerical results associated with macroscopic measurements. We believe that microscopic observations (for example using microsensor technology) of the porous systems with changing saturation dynamics will provide closer and better insight to understand the

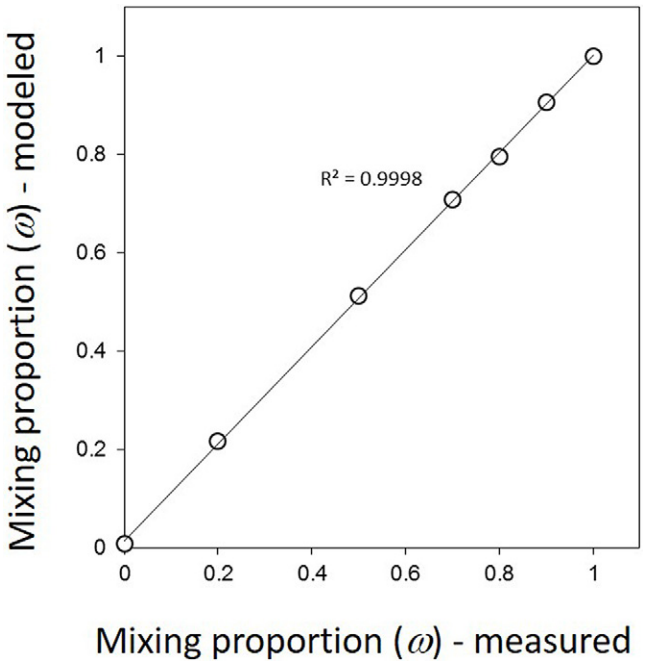

Fig. 4. Measured and model-simulated (Eq. [2]) volumetric mixing proportions (w).

critical changes in thermal behavior in the vicinity of S_0 and S_f. Nevertheless, the improved model (Eq. [8–12]) and the proposed parameters in Table 3 can be conveniently used when predictions are made for the desired mixtures.

Gas Diffusivity

The measured gas diffusivity data across different moisture (saturation) levels are available for limited binary mixtures as illustrated in Fig. 8. The data are shown as average values and the standard deviations ($n = 3$) by the error bars. Note that the gas diffusivity data are scattered in the wet region ($\varepsilon < 0.5$ cm^3 cm^{-3}) due to the presence of high water-induced effects. This intrinsic scatter (due to the random breakdown and formation of capillary bridges across grains) makes it difficult to distinguish any texture-induced effects in gas diffusivity in the wet region. Close observations, however, show that diffusivity for low-porosity binary mixtures (C8F2 and C5F5) is higher than that for high-porosity mixtures (C0F10, C2F8, and C10F0). This corroborates with observations in past studies, for example, by Chamindu Deepagoda et al. (2010), who revealed that, at a given air-filled porosity (ε), high-density soils yielded higher diffusivity than low-density soils due the pronounced water-induced effect on gas diffusivity in low-density soils, irrespective of the soil texture. In general, the effects of soil texture or the different mixing proportions in the binary mixture on D_p/D_o were not particularly apparent in the measured data, as also highlighted in the literature (e.g., Chamindu Deepagoda et al., 2016). In fact, other controlling parameters (e.g., soil density, the presence of macropores) may mask the texture-induced changes in a characteristic D_p/D_o vs. ε relation (Masís-Meléndez et al., 2015). In numerical characterization, therefore, we considered the overall diffusivity data together with the combined Buckingham–Penman modeling approach (Eq. [15]). The original Penman (1940) model with $A = 0.66$ and $B = 1$ provided an upper limit estimate (a safe limit with respect to risk-based analysis) mostly for the wet soils ($\varepsilon \leq 0.5$ cm^3 cm^{-3}), while a model with $A = 1.66$ and $B = 2$ provided an average estimate for the dry soils ($\varepsilon > 0.5$ cm^3 cm^{-3}). Similarly, a useful lower limit descriptive model can be obtained by assigning $A = 3.5$ and $B = 3$.

Analogy between Thermal Conductivity and Gas Diffusivity

By combining these observations on heat and gas transport, Fig. 9 shows in a two-dimensional color contour map the variation of thermal conductivity (in contours) and gas diffusivity (in solid lines) across saturation under varying volume fractions in binary mixtures. The black and white lines represent simulated gas diffusivity (Eq. [15]) contours using the average ($A = 1.66$ and $B = 2$) and lower limit ($A = 3.5$ and $B = 3$) models (Fig. 7), respectively. It is evident that the

Table 3. Numerical characterization or parameterization of the binary mixtures based on grain-size distribution, thermal conductivity, and gas diffusivity.

Porous medium†	Bimodal grain-size distribution (Eq. [2])					Thermal conductivity (improved Côté–Konrad model parameters, Eq. [9] and [11–12])			
						Region 1		Region 2	
	α_c	β_c	α_f	β_f	w	S_o	S_f	λ_f	k
	mm		mm					W m^{-1} K^{-1}	
C10F0	1.09	10.0	–	–	1.00	0.009	0.060	2.32	17.0
C9F1	1.09	9.95	0.139	4.15	0.906	0.039	0.095	2.87	3.16
C8F2	1.08	10.0	0.155	3.91	0.794	0.038	0.150	3.45	0.85
C7F3	1.09	9.79	0.149	4.52	0.709	0.020	0.125	3.74	2.42
C5F5	1.09	9.59	0.149	4.54	0.512	0.002	0.140	3.55	2.80
C2F8	1.08	8.54	0.149	4.52	0.218	0.021	0.088	2.69	1.86
C0F10	–	–	0.150	4.41	0.009	0.004	0.088	2.02	6.69

† Mixtures are named as the ratio of coarse (C) to fine (F) grain size.

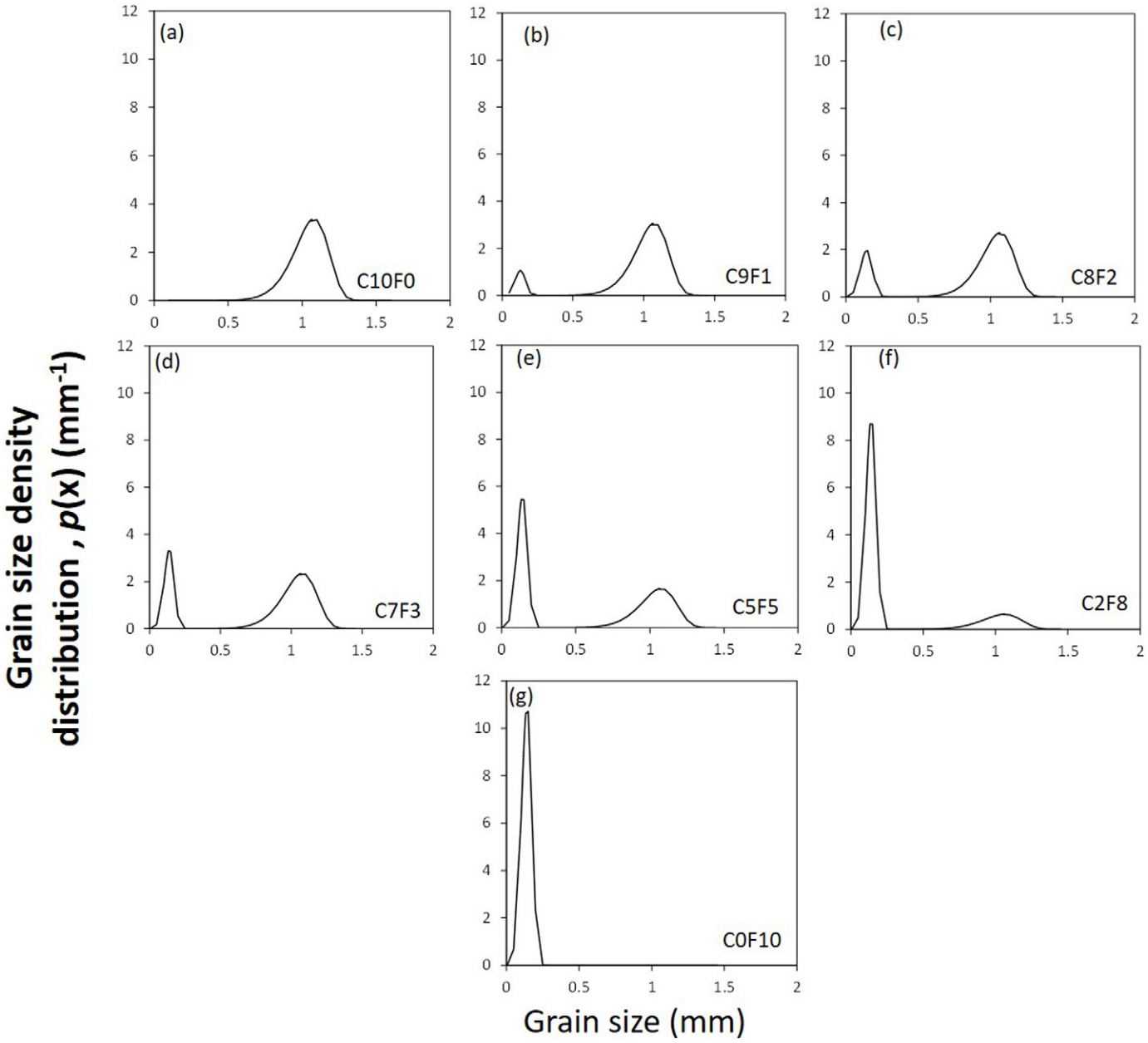

Fig. 5. The grain-size density function, $p(x)$ (Eq. [3] and [4]), for seven different binary sand mixtures named as the ratio of coarse (C) to fine (F) grain size.

responses of thermal conductivity and gas diffusivity to the volumetric fraction of sand mixtures follow similar patterns, demonstrating a strong analogy between the gas diffusivity and thermal conductivity in binary mixtures across saturation conditions. Both contour patterns show a minimum at a volumetric fraction of 0.3, where the total porosity is minimum, implying strong porosity-dependence of the two transport properties. However, the steep gradients in thermal conductivity contours reveal strong dependence of thermal conductivity on the solid fraction compared with the mild gradients of contours in gas diffusivity, which is more an air-filled porosity dependent parameter. At very small saturations ($S < 0.05$), both thermal conductivity and gas diffusivity are less solid-fraction-dependent, although the gas diffusivity contours do not truly reflect it due to the difficulty in numerically characterizing gas diffusivity at very low saturation (see Fig. 8). Importantly, the figure can be used as a tool to determine the required volume fraction and saturation to obtain an expected thermal conductivity and gas diffusivity in an engineering or research application (e.g., in a customized gas-thermal heat exchanger) where the two sand grades are used.

Overall, this study provided insightful experimental and numerical observations on physical, thermal, and gas diffusion properties in the selected seven volumetric mixtures of the two differently textured sand grades. We presented detailed numerical characterization when observed data showed distinct texture-induced effects (e.g., GSD and thermal conductivity), while a general approach was followed when texture-induced effects were

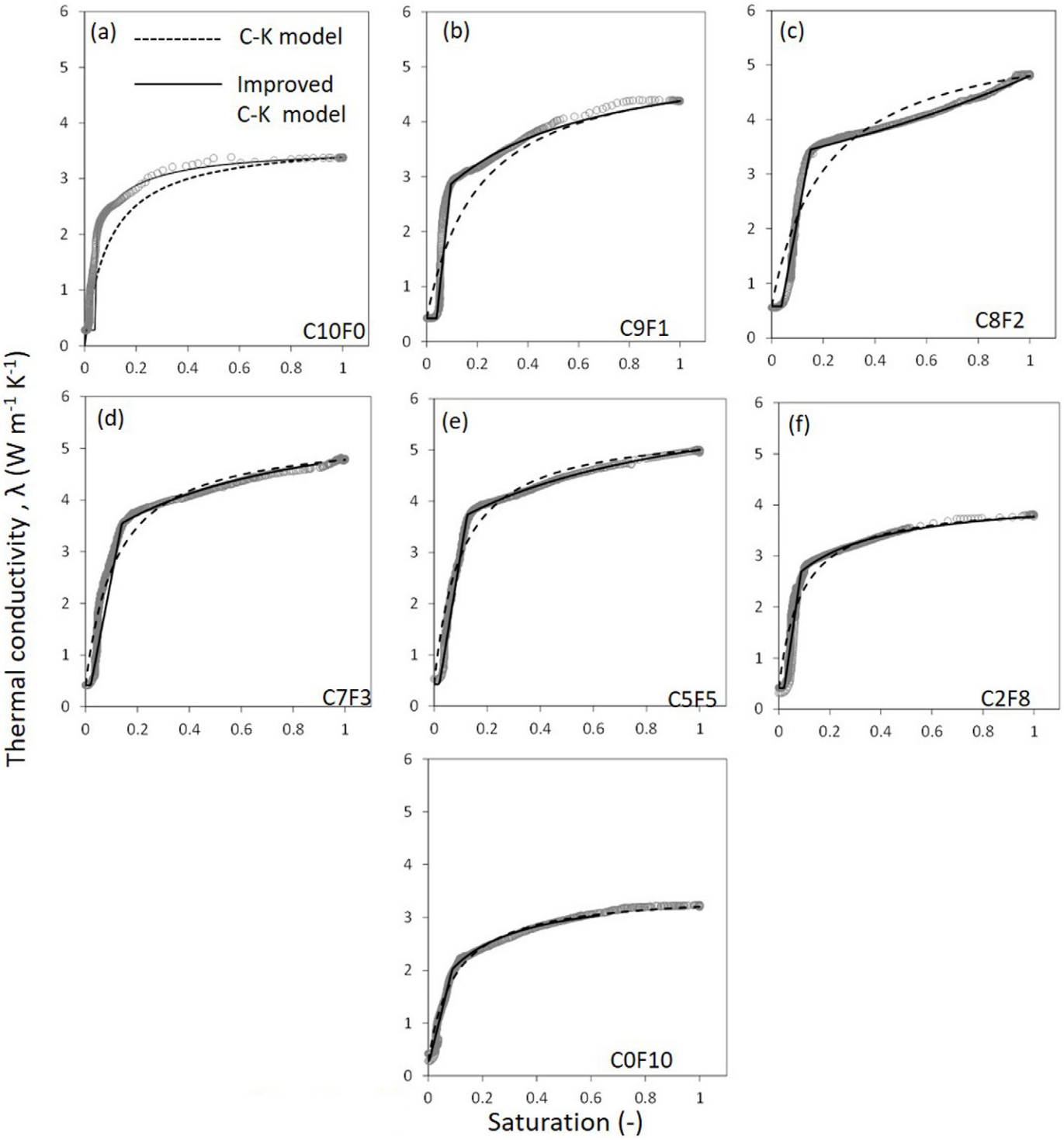

Fig. 6. Measured thermal conductivity (λ) as a function of saturation (*S*) for seven different binary sand mixtures named as the ratio of coarse (C) to fine (F) grain size. Model simulations using the Côté and Konrad (2005) model (Eq. [9], dotted line), and improved Côté and Konrad model (Eq. [10–12], solid line) are also shown.

not dominant within the high-variability data (e.g., gas diffusivity). Although the models presented here are essentially descriptive in nature and involve a number of fitting parameters, the parametric functions can be applied to other differently textured sand grains and also for (extended) multicomponent mixtures with only limited measurements.

Conclusions

This study investigated the GSD, thermal conductivity, and gas diffusivity of seven volumetric mixtures of two differently textured silica sand grades. We extended the classical parametric Rosin and Rammler (1933) GSD function to characterize the bimodal (two-region) behavior in size distribution for binary

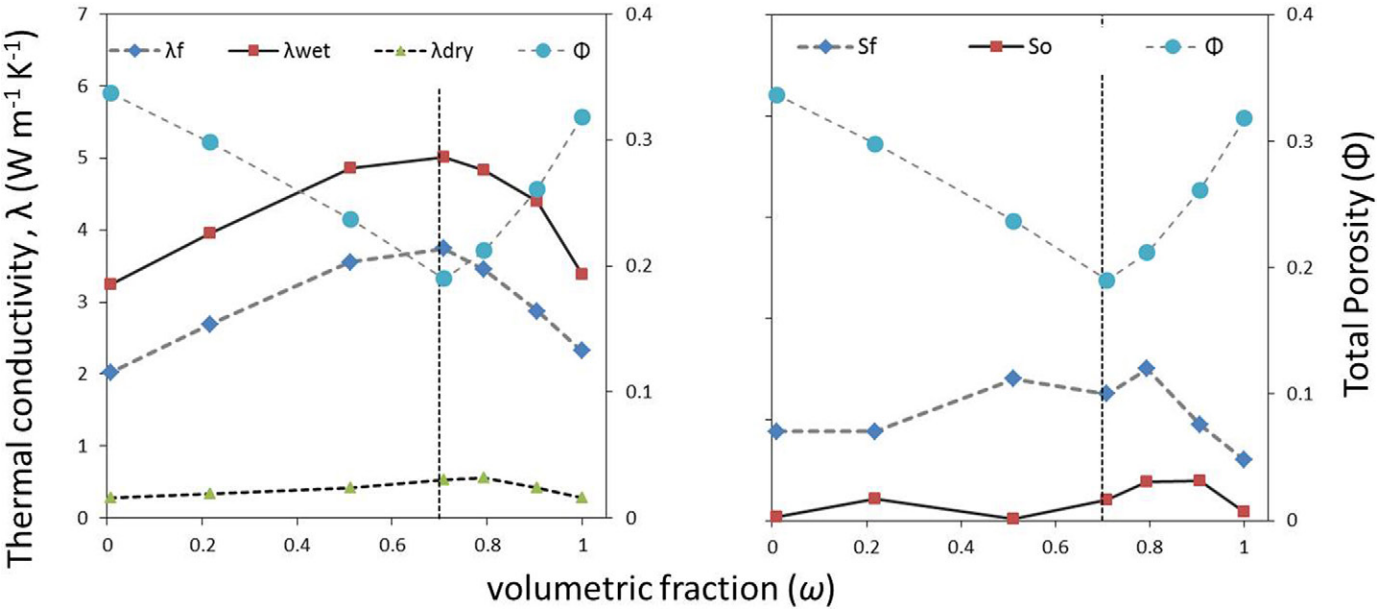

Fig. 7. Variation of three measured and simulated thermal conductivity (λ) values—fully water saturated (λ_{sat}), completely dry (λ_{dry}) (Table 1), and at the saturation that marks the termination of the sharp increase in thermal conductivity (λ_f) (Eq. [9])—as a function of volumetric proportion (w), and the variation in total porosity (Φ) as a function of w (the secondary y axis) (left); and two simulated parameters, S_0 and S_f (Eq. [9–11]), as a function of w and of total porosity (Φ) (the secondary y axis) (right).

mixtures. The extended GSD function accurately described the measured bimodal size distribution with highly consistent parameters and thus showed the applicability of the concept for multimodal GSDs as well. Under a given saturation, the measured thermal conductivity peaked when the porosity of the binary mixture was minimum, thus emphasizing the role of grain-to-grain contacts in porous media heat transfer. We used the Côté and Konrad (2005) thermal conductivity model, and also the recently introduced and improved C-K model (Chamindu Deepagoda et al., 2016), to adequately describe the distinct three-region characteristics in observed thermal conductivity–saturation relations

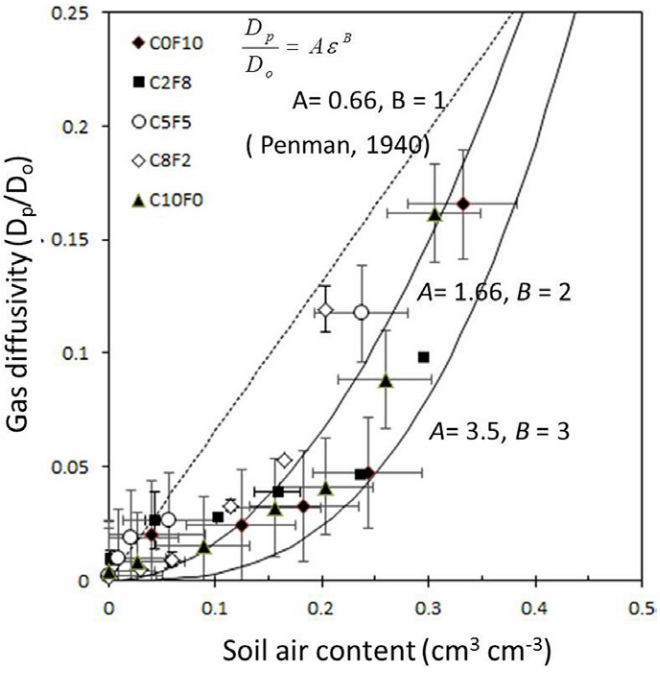

Fig. 8. Gas diffusivity (D_p/D_o) as a function of air-filled porosity (ε) for the five differently textured sand types named as the ratio of coarse (C) to fine (F) grain size. The combined Buckingham–Penman model (Eq. [15]) descriptions are also shown for (i) upper limit (dotted line), (ii) average (solid line), and (iii) lower limit (dashed–dotted line) scenarios.

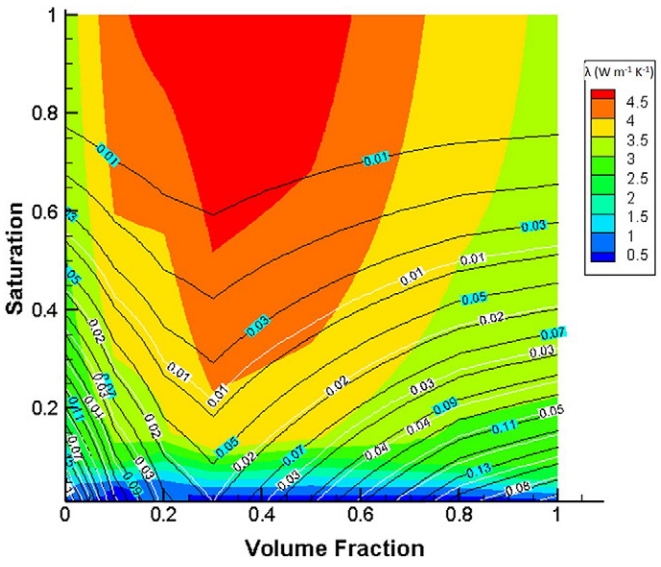

Fig. 9. Contour map showing the thermal conductivity (λ) and gas diffusivity (D_p/D_o) across different volume fractions of sand mixtures (x axis) and under different saturation conditions (y axis). The color contours denote λ (Eq. [8–12]), while the solid black lines and white lines represent D_p/D_o with average and lower limit predictions (Eq. [15]), respectively.

for binary mixtures. Measured gas diffusivity data did not exhibit distinct effects of mixing differently textured sand grades; however, other induced effects (e.g., density-induced macropores) were apparent. To describe the observed gas diffusivity–air content relations, we used a combined Buckingham–Penman model and presented upper limit, average, and lower limit gas diffusivity across the entire water content. The study thus provides useful parameterized models that can potentially be used in various engineering and research-based applications where heat and gas transfer in different porous medium mixtures are used.

Acknowledgments

This research was funded in part by the Department of Energy's National Energy Technology Laboratory (NETL), the Research Partnership to Secure Energy for America project (no. RFP2012UN001) and the National Science Foundation Project Award no. 1447533. The research grant from the University of Peradeniya, Sri Lanka (URG/2016/33/E), is also acknowledged. Any opinion, findings, and conclusions or recommendations expressed herein are those of the authors and do not necessarily reflect the views of those providing technical input or financial support. The trade names mentioned herein are merely for identification purposes and do not constitute endorsement by any party involved in this study.

References

Abriola, L.M., E.L. Miller, K.D. Pennell, C.A. Ramsburg, and J.A. Christ. 2013. Metric identification and protocol development for characterizing DNAPL source zone architecture and associated plume response. Project ER-1612 final report. US Dep. of Defense Strategic Environ. Res. and Dev. Program, Alexandria, VA.

Buckingham, E. 1904. Contributions to our knowledge of the aeration of soils. Bur. Soil Bull. 25. US Gov. Print. Office, Washington, DC.

Campbell, G.S. 1985. Soil physics with BASIC: Transport models for soil–plant systems. Elsevier, New York.

Campbell, G.S., J.D. Jungbauer, W.R. Bidlake, and R.D. Hungerford. 1994. Predicting the effect of temperature on soil thermal conductivity. Soil Sci. 158:307–313. doi:10.1097/00010694-199411000-00001

Chamindu Deepagoda, T.K.K., P. Moldrup, P. Schjønning, L.W. de Jonge, K. Kawamoto, and T. Komatsu. 2010. Density-corrected models for gas diffusivity and air permeability in unsaturated soil. Vadose Zone J. 10:226–238. doi:10.2136/vzj2009.0137

Chamindu Deepagoda, T.K.K., P. Moldrup, P. Schjønning, K. Kawamoto, T. Komatsu, and L.W. de Jonge. 2011. Generalized density-corrected model for gas diffusivity in variably saturated soils. Soil Sci. Soc. Am. J. 75:1315–1329. doi:10.2136/sssaj2010.0405

Chamindu Deepagoda, T.K.K., K.M. Smits, J. Ramirez, and P. Moldrup. 2016. Characterization of thermal, hydraulic, and gas diffusion properties in variably saturated sand grades. Vadose Zone J. 15(4). doi:10.2136/vzj2015.07.0097

Chen, S.X. 2008. Thermal conductivity of sands. Heat Mass Transf. 44:1241–1246. doi:10.1007/s00231-007-0357-1

Côté, J., and J.M. Konrad. 2005. A generalized thermal conductivity model for soils and construction materials. Can. Geotech. J. 42:443–458. doi:10.1139/t04-106

Currie, J.A. 1960. Gaseous diffusion in porous media: 1. A non-steady state method. Br. J. Appl. Phys. 11:314–317. doi:10.1088/0508-3443/11/8/302

Delavar, M.A., and M. Azimi. 2013. Using porous material for heat transfer enhancement in heat exchangers: Review. J. Eng. Sci. Technol. Rev. 6(1):14–16.

Delhoménie, M.C., and M. Heitz. 2005. Biofiltration of air: A review. Crit. Rev. Biotechnol. 25:53–72. doi:10.1080/07388550590935814

de Vries, D.A. 1963. Thermal properties of soils. In: W.R. van Wijk, editor, Physics of plant environment. North-Holland, Amsterdam. p. 210–235.

Dias, R.P., J.A. Teixeira, M.G. Mota, and A.I. Yelshin. 2004. Particulate binary mixtures: Dependence of packing porosity on particle size ratio. Ind. Eng. Chem. Res. 43:7912–7919. doi:10.1021/ie040048b

DiCarlo, D.A. 2004. Experimental measurements of saturation overshoot on infiltration. Water Resour. Res. 40:W04215. doi:10.1029/2003WR002670

Donaldson, E.C., E.V. Chilingarian, and T.F. Yen. 1985. Enhanced oil recovery. I: Fundamentals and analyses. Elsevier, Amsterdam.

Haigh, S.K. 2012. Thermal conductivity of sands. Geotechnique 62:617–625. doi:10.1680/geot.11.P.043

Hamamoto, S., P. Moldrup, K. Kawamoto, and T. Komatsu. 2009. Effect of particle size and soil compaction on gas transport parameters in variably saturated, sandy soils. Vadose Zone J. 8:986–995. doi:10.2136/vzj2007.0144

Hamamoto, S., P. Moldrup, K. Kawamoto, T. Sakaki, T. Nishimura, and T. Komatsu. 2016. Pore network structure linked by X-ray CT to particle characteristics and transport parameters. Soils Found. 56:676–690. doi:10.1016/j.sandf.2016.07.008

Johansen, O. 1975. Thermal conductivity of soils. Ph.D. diss. Norwegian Univ. of Science and Technol., Trondheim (CRREL Draft Transl. 637, 1977).

Lemaitre, J., J.P. Troadec, D. Bideau, A. Gervois, and E. Bougault. 1988. The formation factor of the pore space of binary mixtures of spheres. J. Phys. D: Appl. Phys. 21:1589–1592.

Lu, N., and Y. Dong. 2015. Closed-form equation for thermal conductivity of unsaturated soils at room temperature. J. Geotech. Geoenviron. Eng. doi:10.1061/(ASCE)GT.1943-5606.0001295

Lu, S., T.S. Ren, Y.S. Gong, and R. Horton. 2007. An improved model for predicting soil thermal conductivity from water content. Soil Sci. Soc. Am. J. 71:8–14. doi:10.2136/sssaj2006.0041

Marshall, T.J. 1959. The diffusion of gases through porous media. J. Soil Sci.10:79–82.

Masís-Meléndez, F., L.W. de Jonge, T.K.K. Chamindu Deepagoda, M. Tuller, and P. Moldrup. 2015. Effects of soil bulk density on gas transport parameters and pore-network properties across a sandy field site. Vadose Zone J. 14(7). doi:10.2136/vzj2014.09.0128

Millington, R.J. 1959. Gas diffusion in porous media. Science 130:100–102. doi:10.1126/science.130.3367.100-a

Millington, R.J., and J.M. Quirk. 1960. Transport in porous media. In: F.A. Van Beren et al., editors, Transactions of the 7th International Congress of Soil Science, Madison, WI. 14–21 Aug. 1960. Elsevier, Amsterdam. p. 97–106.

Millington, R.J., and J.M. Quirk. 1961. Permeability of porous solids. Trans. Faraday Soc. 57:1200–1207. doi:10.1039/tf9615701200

Moldrup, P., T. Olesen, J. Gamst, P. Schjønning, T. Yamaguchi, and D.E. Rolston. 2000. Predicting the gas diffusion coefficient in repacked soil: Water induced linear reduction model. Soil Sci. Soc. Am. J. 64:1588–1594. doi:10.2136/sssaj2000.6451588x

Mota, M., J.A. Teixeira, W.R. Bowen, and A. Yelshin. 2001. Binary spherical particle mixed beds: Porosity and permeability relationship measurement. Trans. Filtr. Soc. 1:101–106.

Pavel, B.I., and A.A. Mohamad. 2004. An experimental and numerical study on heat transfer enhancement for heat exchangers fitted with porous media. Int. J. Heat Mass Transfer 47:4939–4952. doi:10.1016/j.ijheatmasstransfer.2004.06.014

Penman, H.L. 1940. Gas and vapor movements in soil: The diffusion of vapors through porous solids. J. Agric. Sci. 30:437–462. doi:10.1017/S0021859600048164

Pokhrel, D., P. Hettiaratchi, and S. Kumar. 2011. Methane diffusion coefficient in compost and soil–compost mixtures in gas phase biofilter. Chem. Eng. J. 169:200–206. doi:10.1016/j.cej.2011.03.013

Rolston, D.E., and P. Moldrup. 2002. Gas diffusivity. In: J.H. Dane and G.C. Topp, editors, Methods of soil analysis. Part 4. SSSA Book Ser. 5. SSSA, Madison, WI. p. 1113–1139. doi:10.2136/sssabookser5.4.c45

Rosin, P., and E. Rammler. 1933. Laws governing the fineness of powdered coal. J. Inst. Fuel 7:29–36.

Sakaki, T., and T.H. Illangasekare. 2007. Comparison of height-averaged and point-measured capillary pressure–saturation relations for sands using a modified Tempe cell, Water Resour. Res. 43:W12502. doi:10.1029/2006WR005814

Sakaki, T., and K.M. Smits. 2015. Water retention characteristics

and pore structure of binary mixtures. Vadose Zone J. 14(2). doi:10.2136/vzj2014.06.0065

Schjønning, P. 1985. A laboratory method for determination of gas diffusion in soil. (In Danish, with English summary.) Rep. S1773. Danish Inst. of Plant and Soil Sci., Tjele.

Schroth, M.H., S.J. Ahearn, J.S. Selker, and J.D. Istok. 1996. Characterization of Miller-similar silica sands for laboratory hydrologic studies. Soil Sci. Soc. Am. J. 60:1331–1339. doi:10.2136/sssaj1996.03615995006000050007x

Smits, K.M., T. Sakaki, S.E. Howington, J.F. Peters, and T.H. Illangasekare. 2012. Temperature dependence of thermal properties of sands across a wide range of temperatures (30–70°C). Vadose Zone J. 12(1). doi:10.2136/vzj2012.0033

Smits, K.M., T. Sakaki, A. Limsuwat, and T.H. Illangasekare. 2010. Thermal conductivity of sands under varying moisture and porosity in drainage–wetting cycles. Vadose Zone J. 9:172–180. doi:10.2136/vzj2009.0095

Sweijen, T., H. Aslannejad, and S. Hassanizadeh. 2017. Capillary pressure–saturation relationships for porous granular materials: Pore morphology method vs. pore unit assembly method. Adv. Water Resour. 107:22–31. doi:10.1016/j.advwatres.2017.06.001

Tarnawski, V.R., M.L. McCombie, T. Momose, I. Sakaguchi, and W.H. Leong. 2013. Thermal conductivity of standard sands: III. Full range of saturation. Int. J. Thermophys. 34:1130–1147. doi:10.1007/s10765-013-1455-6

Taylor, C.E., and J.T. Kwan. 2004. Advances in the study of gas hydrates. Kluwer Acad., New York.

Taylor, S.A. 1950. Oxygen diffusion in porous media as a measure of soil aeration. Soil Sci. Soc. Am. Proc. 14:55–61. doi:10.2136/sssaj1950.036159950014000C0013x

Troeh, F.R., J.D. Jabro, and D. Kirkham. 1982. Gaseous diffusion equations for porous materials. Geoderma 27:239–253. doi:10.1016/0016-7061(82)90033-7

Wallen, B.M., K.M. Smits, T. Sakaki, S.E. Howington, and T.K.K. Chamindu Deepagoda. 2016. Thermal conductivity of binary sand mixtures evaluated through full water content range. Soil Sci. Soc. Am. J. 80:592–603. doi:10.2136/sssaj2015.11.0408